Research Square

Preprints are preliminary reports that have not undergone peer review.
They should not be considered conclusive, used to inform clinical practice,
or referenced by the media as validated information.

The Upregulation of Gnao1 in Mesencephalic Astrocytes Triggers Neuroprotective Mechanisms through cAMP/PKA/pCREB in A53T-α-Synuclein Mice

Michele Tufano
University of Naples “Federico II”
Giulia Riso
University of Naples “Federico II”
Maria Josè Sisalli
University of Naples “Federico II”
Rohan Mahesh Patil
University of Naples “Federico II”
Elena D’Apolito
University of Naples “Federico II”
Ester Licastro
University of Naples “Federico II”
Giuseppe Pignataro
University of Naples “Federico II”
Agnese Secondo
Polytechnic University of Marche
Anna Pannaccione
University of Naples “Federico II”
Lucio Annunziato
IRCCS Synlab SDN S.p.A
Antonella Scorziello
scorziel@unina.it

University of Naples “Federico II”

Article

Keywords:

Posted Date: October 22nd, 2026

DOI: https://doi.org/10.21203/rs.3.rs-11266583/v1

License: This work is licensed under a Creative Commons Attribution 4.0 International License.
Read Full License

Additional Declarations: No competing interests reported.

Abstract

Gnao1 encodes $G\alpha_o$, a G protein subunit highly expressed in the striatum that regulates neurotransmission and motor control. While $G\alpha_o$'s neuronal role is established, its function in pathological conditions such as Parkinson's disease (PD) remain largely unexplored. Reanalysing single-nucleus RNA-sequencing data from A53T-α-Syn-transgenic mice, we identified *Gnao1* as selectively upregulated in mesencephalic astrocytes. Longitudinal analysis performed in this model at 4, 12, and 16 months revealed that the *Gnao1* increase was restricted to the midbrain, peaking at 12 months, a stage characterized by reactive astrogliosis and dopaminergic neuronal impairment without overt degeneration. Functional assays in primary mesencephalic astrocytes from A53T-α-Syn transgenic mice demonstrated that *Gnao1* regulates astrocyte-state transition through the cAMP/PKA/pCREB pathway. Interestingly, knocking down of *Gnao1* prevented these effects and shifted astrocytes toward a detrimental phenotype. These findings identify *Gnao1* as a novel regulator of mesencephalic astrocyte transition in a model of PD, suggesting that astrocytic $G\alpha_o$-dependent signalling represents an early adaptive response to neuronal dysfunction.

Introduction

The *Gnao1* gene encodes the $G\alpha_o$ subunit of heterotrimeric G proteins, which is highly expressed in the central nervous system, where it couples with several G protein-coupled receptors (GPCRs), including those for dopamine, GABA, acetylcholine, and opioids[1,2]. $G\alpha_o$ regulates adenylyl cyclase and cyclic AMP (cAMP) production by controlling the availability of Gβγ subunits[3]. In the dopaminergic system, $G\alpha_o$ is a key regulator of D1 and D2 receptor signalling in medium spiny neurons (MSNs): it is required for motor learning through D1 receptor-expressing direct-pathway MSNs and contributes to coordination, balance and movement through D2 receptor-expressing indirect-pathway [3,4]. In Parkinson's disease (PD), the loss of nigrostriatal dopamine deprives MSNs of their primary modulatory input, leading to structural, electrophysiological, and molecular changes that contribute to motor dysfunction[5,6]. Pathogenic variants in *Gnao1* can affect patients differently depending on where the mutation occurs in the gene, causing a spectrum of mild to severe epilepsy, movement disorders, or a combination of both[2,7–9]. Hypotonia, seizures and abnormal involuntary movements are the most common early manifestations [10]. A complex hyperkinetic movement disorder encompassing dystonia, chorea, orofacial dyskinesia, and ballism is observed in most patients, while severe hypotonia and impaired postural control often characterize the early stages of the disease, preceding the onset of overt hyperkinesia[11]. In a subset of patients, paroxysmal dystonic-dyskinetic exacerbations become severe enough to require intensive care and may be life-threatening[10]. In addition to the classic hyperkinetic presentation, milder or atypical phenotypes are increasingly recognized, including late-onset focal or segmental dystonia and parkinsonian features such as bradykinesia and resting tremor, observed in approximately 13% of reported cases[2]. Notably, a recent study demonstrated that mutations specifically targeting the N-terminal α-helix of $G\alpha_o$ cause a distinct hypokinetic phenotype characterized by parkinsonism with

bradykinesia and rigidity, mechanistically linked to the loss of heterotrimeric G-protein formation and impaired GPCR coupling[12]. This finding highlight $G\alpha_o$ is a potential contributor to mechanisms underlying nigrostriatal dysfunction occurring in PD. In this regard, the results obtained by reanalysing a published single-nucleus RNA-sequencing atlas from A53T-α-Syn-transgenic mice[13], a model reproducing a familial form of PD, further support this suggestion. Indeed, we identified *Gnao1* as selectively upregulated in mesencephalic astrocytes. This finding was particularly intriguing, since $G\alpha_o$ has been studied extensively in neurons and linked to motor circuit dysfunction, whereas its role in astrocytes in the context of PD remains largely unexplored. In multiple brain cell types, including astrocytes and oligodendrocytes, $G\alpha_o$ regulates oxidative stress responses, proliferation, growth factor production, and myelination[14,15]. Based on these findings the present study aimed to:

1. Characterize the role of $G\alpha_o$ in mesencephalic astrocytes in the A53T-α-Syn transgenic mouse model.
2. Investigate whether $G\alpha_o$ upregulation represents a compensatory mechanism that regulates astrocytic reactive states and phenotypes.
3. Determine whether astrocytic $G\alpha_o$ signalling promotes adaptive neuroprotective responses to dopaminergic neuronal loss.

To test these hypotheses, we used molecular and biochemical approaches in mice carrying the human A53T mutation of α-Syn. We found that *Gnao1* products are selectively upregulated in mesencephalic astrocytes and may act as a compensatory mechanism through the cAMP/PKA/pCREB pathway. This signalling promotes a neurotrophic astrocytic state and supports dopaminergic neuronal survival against α-Syn aggregation.

Results

In silico analysis revealed Gnao1 is upregulated in mesencephalic astrocytes of A53T-α-Syn transgenic mice

We re-analysed an existing snRNA-sequencing atlas from 6-month-old A53T-α-Syn-Transgenic mice, which represent the prodromal phase of the disease[13]. Examination of the raw data indicated an upregulation of *Gnao1* in mesencephalic astrocytes. Consequently, we compared the expression of A53T-α-Syn-Transgenic mice-dysregulated genes, in mesencephalic and striatal glial cells. Venn diagram analysis identified 399 differentially expressed genes unique to striatal astrocytes and 80 unique genes to mesencephalic astrocytes, while 266 were shared across both regions (Fig. 1A). To gain functional insight into these transcriptional changes, we performed KEGG pathway enrichment analysis, which is presented as bubble plots. The analysis highlighted a strong association with pathways linked to neurodegenerative disorders, including PD, Alzheimer's disease (AD), Huntington's disease (HD), and Amyotrophic Lateral Sclerosis (ALS) (Fig. 1B-C). Notably, astrocytes in midbrain and striatum exhibited dysregulation of genes associated with potentially neurodegenerative activity, suggesting a common

contribution to neurodegenerative processes despite their regional molecular differences. To further investigate regional differences in astrocytic responses, we focused on the 266 genes commonly dysregulated in both mesencephalic and striatal astrocytes. Comparison of the fold-change values between the two regions revealed that 14 genes displayed divergent expression patterns, indicating region-specific regulation despite their shared dysregulation (Fig. 1D). Among these genes, *Gnao1* emerged as particularly interesting because it showed opposite regulation in the two brain regions examined, being upregulated in mesencephalic astrocytes while downregulated in striatal astrocytes (Fig. 1D). Given the established paradigm that microglial-secreted factors, specifically TNF-α, IL-1α, and C1q (TIC)[16–18] are the drivers of the canonical inflammatory astrocyte state, we extended the analysis to other glial populations within the same dataset to determine if the observed astrocytic changes were secondary to microglial activation. Interestingly, the analysis revealed a marked regional divergence in microglial transcriptional responses that did not reflect the astrocytic profile. Indeed, the Venn diagram analysis showed that microglial populations in the two regions exhibited entirely non-overlapping sets of dysregulated genes (87 unique to the midbrain and 48 to the striatum) with no shared genes between the two populations (Figure S1A). This contrast to the 266 genes shared by astrocytes suggests that the glial response in the A53T-α-Syn-Transgenic mice model is highly cell-type and region-dependent. KEGG pathway enrichment analysis was found exclusively in striatal microglia, mainly involving genes linked to PD susceptibility (Figure S1B). Conversely, oligodendrocytes showed a more synchronized response across regions; we identified 169 dysregulated genes in the midbrain and 328 in the striatum (Figure S1C), with a correlation analysis confirming a linear relationship between their regional expression changes (Figure S1D). Like astrocytes, OLGs in both regions exhibited dysregulation of genes associated with neurodegenerative pathways (PD, HD, and ALS) and potentially neurotoxic functions (Figure S1E-F). These findings collectively suggest that in the A53T-α-Syn-Transgenic mice, the classic "TIC" theory of astrocyte activation proposed by Barres and Liddelow[16–18] is not strictly recapitulated. The absence of a shared, robust inflammatory signature in microglial cells across both regions coupled with the highly specific upregulation of *Gnao1* exclusively in mesencephalic astrocytes indicates that the astrocytic reactivity in this mice model of PD may be driven by cell-intrinsic mechanisms or alternative signalling rather than a microglial trigger.

Gnao1 products are upregulated in the midbrain of 12-Month-old A53T-α-Syn-transgenic mice

To validate the *in-silico* data and characterize the expression of *Gnao1* we performed qPCR and Western blot in the midbrain and striatum of A53T-α-Syn-Transgenic mice at 4-12-, and 16-months of age corresponding to the prodromal, intermediate, and late stages of the disease, respectively (Fig. 2).

We found that *Gnao1* and $G\alpha_o$ upregulation occurred specifically in the midbrain of A53T-α-Syn-Transgenic mice at 12 months compared with age-matched controls (Fig. 2A-B). No differences in *Gnao1* gene and $G\alpha_o$ protein expression were observed in the striatum of A53T-α-Syn-Transgenic mice at all the time points examined (Fig. 2C-D). To further confirm the regional specificity of this increase, we

performed additional Western blot analyses in the cortex and cerebellum of 12-month-old mice and found that levels of $G\alpha_o$ protein did not differ compared to controls (Fig. 2E-F).

Gnao1 products overexpression is associated with cAMP/PKA/CREB activation in primary mesencephalic astrocytes obtained from A53T-α-Syn-Transgenic mice

To validate the findings obtained in the A53T-α-Syn-Transgenic mouse model and to assess both the specificity of the observed alteration for mesencephalic astrocytes and the effects of *Gnao1* upregulation, we next moved to an *in vitro* model. We performed qPCR, Western blotting, and immunofluorescence analysis on primary astrocytes derived from the midbrain, striatum, cortex and cerebellum of WT and A53T-α-Syn-Transgenic mice (Fig. 3). Our results demonstrated that A53T mesencephalic astrocytes displayed elevated *Gnao1 and* $G\alpha_o$ protein expression compared to WT controls (Fig. 3A-C). Conversely, no differences in *Gnao1* gene and $G\alpha_o$ protein expressions were observed in astrocytes obtained from striatum, cortex and cerebellum (Fig. 3D-L). The $G\alpha_o$ subunit is a key regulator of cAMP. Given its specific increase in the A53T mesencephalic astrocytes, we explored the involvement of the canonical cAMP/PKA pathway. Interestingly, ELISA assays uncovered a significant increase in basal cAMP levels in A53T mesencephalic astrocytes (Fig. 4A). Furthermore, Western blot analysis of downstream PKA targets confirmed increased levels of phosphorylated CREB (pCREB) in these cells (Fig. 4B), suggesting a complex dysregulation of canonical G-protein signalling in this pathological context. To further characterize the specific phenotype of these mesencephalic astrocytes, we evaluated the expression of a panel of genes representative of reactive versus homeostatic astrocytic activity via qPCR, based on established activation profiles[19–31].The resulting data indicated that A53T mesencephalic astrocytes preferentially express markers associated with an adaptive reactive state while fully preserving the capability to produce neurotrophic factors (Fig. 4C).

Silencing of Gnao1 in primary cultures of mesencephalic astrocytes impaired growth factor production

To confirm the role of *Gnao1* in modulating astrocytic reactivity, we performed silencing experiments using an optimized siRNA concentration (50nM) (Fig. 4D-E; Figure S6C-E). qPCR analysis of reactivity-associated markers revealed that *Gnao1* downregulation induced a transition toward a more pronounced reactive phenotype. This was characterized by the significant upregulation of inflammatory signatures in both WT and A53T astrocytes transfected with siRNA against *Gnao1* (Fig. 4F). To confirm the relationship between *Gnao1* and neuroinflammation, we treated primary WT mesencephalic astrocytes with LPS. We observed a significant downregulation of both Gnao1 and trophic factors, alongside an increased expression of genes linked to a detrimental astrocytic phenotype (Fig. 4F). Prompted by these in vitro findings and the initial transcriptomic data showing marked regional differences in glial responses, we next investigated how these distinct astrocytic and microglial phenotypes evolved in A53T-α-Syn-Transgenic mice during disease progression. We analysed a panel of glial markers at prodromal (4 months), intermediate (12 months), and late (16 months) stages of the diseases. Astrocytic state was evaluated using markers representative of cellular reactivity like CXCL10, GFAP, C3, Amigo2 and Serping1 and physiological/adaptive activity like S100A10, CD14, PTX3 and SOX9[19–31].

Microglial subpopulations were characterized using IBA-1, CD68, CD86, C1Q, iNOS, TNFα, IL-1β, and CD206 as reactive/pro-inflammatory markers, and CD206 as neuroprotective/alternative activation marker[32–35]. In the midbrain of A53T-α-Syn-Transgenic mice, qPCR results showed an age-related increase in reactive astrocyte markers compared with WT controls, whereas no significant changes were detected in microglial markers (Fig. 5A). Conversely, the striatum of transgenic mice displayed a progressive increase in detrimental microglial markers over time, while astrocytic markers remained unchanged compared with WT mice (Fig. 6A). These regional transcriptional profiles were fully validated by Western blot and immunohistochemical analyses. While 4-month-old A53T-α-Syn-Transgenic mice showed no evidence of glial reactivity or neuroinflammation in the midbrain (Fig. 5B-E), an age-related upregulation of GFAP, C3 and S100A10 protein expression emerged at 12 months and reached statistical significance at 16 months compared to age-matched WT mice (Fig. 5B-E; Figure S2A-B; Figure S3A-B). In contrast, the striatum of A53T-α-Syn-Transgenic mice exhibited a clear predominance of neurotoxic microglial subpopulations, evidenced by increased CD86 expression at both 12- and 16-month (Fig. 6D-E; Figure S4A-B; Figure S5A-B). Taken together, these data revealed a clear, region-specific divergence in glial behaviour starting at 12 months: reactive astrogliosis predominated in the midbrain, whereas a neurotoxic microglial profile characterized the striatum during the later stages of pathology in A53T-α-Syn-Transgenic mice. Finally, we performed immunofluorescence-based cell counting in the SNpc to correlate this regional glial activation with dopaminergic integrity. Given that failing dopaminergic neurons, before undergoing cell death, enter a functionally “silent” state characterized by a reduction in their activity and, consequently, in the expression of tyrosine hydroxylase (TH)[36] we co-assessed TH and DOPA decarboxylase (DDC) expression in our animal model. At 12 months, A53T-α-Syn-Transgenic mice displayed a “silent” dopaminergic phenotype in the SNpc, characterized by significantly reduced TH levels but preserved DDC expression (Fig. 5F). By 16 months, however, both markers were drastically reduced, confirming definitive dopaminergic neurodegeneration (Fig. 5G).

Methods

Animals

Mice expressing the human A53T α-Syn mutation under the control of a prion promoter (Pmp SNCA*A53T) were obtained from The Jackson Laboratory. Mice hemizygous for the α-Syn A53T mutation were bred on a mixed C57Bl/6 × C3H background to produce transgenic and non-transgenic littermates. To identify A53T-α-Syn-Transgenic mice, PCR was performed according to the protocol provided by The Jackson Laboratory. All mice were housed in groups of 1–5 in temperature- and humidity-controlled rooms under a 12-hr light/dark cycle and fed ad libitum with standard mouse chow. Experiments were performed according to international guidelines for animal research. All experiments were performed following the Guide for the Care and Use of Laboratory Animals and approved by the Animal Care Committee of “Federico II”, University of Naples, Italy, Authorization n° 588/20; 658/24 -PR. In line with articles previously published by this laboratory and with the literature, male mice aged 4months were used as a model of the prodromal phase of PD, and male mice aged 12 and16 months

were used as a model reproducing the intermediate and late stage of the disease. Sample size for each experimental group was determined by G*Power software. Given the high intrinsic biological variability characteristic of this animal model, an initial cohort of 24 mice per time point (total n = 96) was planned. However, due to the pronounced aggressiveness typical of this model, 20 mice died from natural causes. The final experimental cohorts were therefore distributed as follows:

Histological and Molecular Profiling (RT-qPCR and Immunofluorescence): 8 animals per time point were analyzed (4, 12, and 16 months).

Protein Expression Analysis (Western Blot): A total of 52 mice were used for Western blot analysis across the three time points (4, 12, and 16 months).

Astrocyte Isolation: cortical, striatal, mesencephalic, and cerebellar astrocytes were isolated from pups (A53T α-Syn and WT pups) across 13 independent dissections.

Primary Astrocyte Cultures from A53T-α-Syn-Transgenic and Wild-Type Mice

Primary Astrocyte Cultures from A53T α-Syn and WT mice were obtained from the midbrain and striatum of new-born 1–2 days old. Proper sterile techniques were kept throughout the culture process. All culture media and soluble components were filter-sterilized before use. Dissection tools were regularly stored in 70% ethanol (EtOH) until use and rinsed with dissection medium (DM) containing Hanks' Balanced Salt Solution (HBSS) 1X. Dissection was performed with different sets of tools to minimize contamination risks, following established protocols[37]. Specifically, after decapitation, the skull skin was removed with forceps, and brain tissue isolation performed under a binocular microscope (Zeiss Stemi DV4 Stereo Microscope). Each animal's midbrain, striatum, cortex and cerebellum were aseptically dissected. Curved forceps were carefully used to remove the meninges and visible blood vessels, to prevent meningeal fibroblasts and endothelial cells contamination. The tissues were minced finely, enzymatically (0.25% trypsin and DNase/MgSO4 37°C, 30 min) and mechanically dissociated to produce single cells suspension. Then the cell suspension was centrifuged at 1000 r.p.m. for 5 min and suspended in DMEM containing 100U/mL penicillin, 100 µg/mL streptomycin and 10% FBS. The cells were plated in 60mm petri dishes, then cultured at 37°C in a 95% air 5% CO2 incubator. The day after plating, genotyping was performed. The medium was changed every two days. When cells reached the confluence after 7–8 days in vitro (DIV), the petri dishes were shaken with PBS 1X for three-times to separate Type 1 astrocytes that were maintained in culture for 14 days (DIV) and then used for the experimental procedures. For Western blotting and Real time PCR experiments astrocytes were cultured in 100 mm petri dishes at 37°C in a humidified 5% CO2 atmosphere, for confocal microscopy experiments and immunocytochemistry cells were plated on glasses pre-coated with Poly-D-Lys. To verify the quality and purity of the astrocytic dissection we used western blot analysis and immunocytochemistry (Figure S6A-B).

Genotyping

DNA was extracted from tail tissue using the manufacturer's instructions (MyTaq Extract-PCR Kit Meridian Bioscience). To identify A53T mice, PCR was performed by preparing a reaction mixture consisting of 1X MyTaq HS mix (MyTaq Extract-PCR Kit Meridian Bioscience), 1µL DNA extract, 1µM internal control primer (FWD:5'-CTAGGCCACAGAATTGAAAGATCT-3', REV: 5' GTAGGTGGAAATTCTAGCATCATCC-3'), 0.5 µM Tg (Prnp-SNCA*A53T)83Vle primer (FWD: 5'-TGTAGGCTCCAAAACCAAGG-3', REV: 5'-TGTCAGGATCCACAGGCATA-3') and water. The primers sequence was provided by Jakson Laboratory (Synthesis Scale: 0.01µmol; Purification: HPSF). Reactions were incubated at 95°C for 3 minutes, followed by thirty-five cycles of 95°C for 15 seconds, 60°C for 15 seconds and 72°C for 30 seconds (Applied Biosystems SimpliAmp Thermal Cycler). After PCR, the samples were loaded onto a 2% (W/V) agarose gel made in 1X Tris acetate-EDTA buffer (40 mM Tris pH 7.6, 20 mM acetic acid, 1 mM EDTA) with SYBR™ Safe DNA Gel Stain (1:10000). DNA was visualised using a UV transilluminator ChemiDoc™ System with Quantity One™ Software (Bio-Rad).

Biochemical analysis

For biochemical analysis, the brains were removed and divided into two equal parts: half of each was frozen in dry ice and used for Western blot analysis. The other halves were fixed in 4% (w/v) paraformaldehyde (PFA) in phosphate-buffered saline (PBS) 1x for immunolabelling assay. For Western blot experiments striatum and midbrain regions were isolated and homogenized in a Dounce Tissue Grinder (Avantor VWR) with RIPA Buffer containing Tris HCL 50mM, pH 7.4; NaCl 150mM; Triton X-100 1%; Sodium deoxycholate 0.5%; SDS 0.1%; EDTA 1mM; NaF 10mM; PMSF 1mM; Na3VO4 1 mM and protease inhibitor cocktail Roche. Homogenates were centrifuged at 10,000 rpm for 20 minutes at 4°C and the supernatants were collected in -80°C. Protein concentrations were identified using Bradford method (#5000001 Protein Assay Dye Reagent Concentrate, BioRad). For analysis 30 µg of proteins from tissue lysates and 10 µg from cell lysates were separated on 8% or 12% sodium dodecyl sulphate-polyacrylamide gels with 5% sodium dodecyl sulphate stacking gel (SDS-PAGE) and electro-transferred onto Hybond ECL nitrocellulose paper (CAT.GE10600001 Amersham, Milan, Italy). The membranes were blocked for 1 hour at room temperature (RT) in a 3% BSA buffer (Merck CAT. A9418) in TBS with 0.1% Tween®20 (Merck CAT.9005-64-5), then incubated with the primary antibodies overnight at 4°C. Rabbit anti-$G\alpha_o$ (1:1000, PA5-3004, Invitrogen), Rabbit anti-$G\alpha_o$ (1:1000, 3975, Cell Signaling), Rabbit anti-GFAP (1:1000, ab7260 Abcam), rabbit anti-IBA-1 (1:1000, ab178846 Abcam), rat anti-C3 (1:500 ab11862 Abcam), rabbit anti-CD86 (1:1000, Genentech), rabbit anti-CREB (1:1000 #4820 Cell Signaling), rabbit anti- phosphorylated CREB(1:1000, 9198 Cell Signaling), rabbit anti-CD31 (1:1000, GTX130274 Genentech), mouse anti-β-actin conjugated with HRP (1:10000, A3854, Sigma Aldrich). Next, all membranes were washed 3 times with a solution containing Tween 20 (0.1%) and subsequently incubated with the secondary antibodies for 1 hour (1:5000) at room temperature (anti-rabbit IgG, HRP-linked, mouse IgG HRP-linked NA931V, Amersham Goat anti-Rat IgG Secondary Antibody, HRP 62-9520

Invitrogen). Immunoreactivity was detected by chemiluminescence kit (ChemiDoc imaging system Bio-Rad), and bands quantified by densitometry using ImageJ software.

Immunofluorescence analysis on brain slices and primary astrocytes.

Mice brains were fixed in 4% PFA in PBS 1x for 24 hours at 4°C. Fixed brains were cryoprotected in 30% (w/v) sucrose in PBS at 4°C until they sank, then sectioned coronally using a cryostat (Slee medical cryostat mev&mnt) to obtain 30 µm thick free-floating sections. Regularly spaced sections (30 µm thickness) at multiple rostro caudal levels were selected to sample the SNpc and the striatum (caudate putamen CPu). Specifically, SNpc sections were selected according to the following anteroposterior coordinates relative to bregma[38,39] −2.92, − 3.08, − 3.16, − 3.28, and − 3.40 mm. Corresponding sections from WT and A53T animals were matched for each coordinate. Identification of the SNpc was based on both the mouse brain atlas[39]. Similarly, striatal (CPu) sections were collected at anteroposterior coordinates: 1.18, 1.10, 0.98, 0.86, and 0.62 mm from bregma[38]. For immunofluorescence staining, free-floating sections were washed three times in PBS 1x and subsequently permeabilized in PBS 1x containing 0.1% Triton X-100 for 1 hour at room temperature (RT). After permeabilization, sections were incubated for 1 hour at RT in blocking solution (PBS 1x, 0.1% Triton X-100, and 0.1% of BSA). Primary antibody incubation was performed overnight at 4°C with the following antibody mixture prepared in PBS 1x with 1% BSA: rat anti-C3 (1:200, Abcam, ab11862), mouse anti-GFAP (1:500, Thermo Fisher Scientific, 14-9892-82), rabbit anti-S100A10 (1:500, Invitrogen, PA5-95505), rat anti-IBA-1 (1:500 wako, 01919741), rabbit anti-CD86 (1:200, GTX32507 Genentech). The next day, sections were incubated for 1 hour at RT in the corresponding secondary antibody mixture prepared in PBS 1x containing 0.1% BSA: goat anti-rat Alexa Fluor 647 (1:200, Invitrogen, A-21247), goat anti-mouse Alexa Fluor 488 (1:500, Invitrogen, A11001), and goat anti-rabbit Alexa Fluor 555 (1:200, Invitrogen, A-21428), goat anti-rabbit Alexa Fluor 488 (1:200, Invitrogen, A11001). After incubation, sections were washed three times in PBS 1x and mounted on microscope slides using an aqueous mounting medium with DAPI (Fluoroshield™ with DAPI, Sigma, F6057-20ML). Slides were stored at 4°C in the dark until imaging. For each stained section at the level of the SNpc and CPu, five images were acquired using a confocal microscope (Zeiss LSM 700) at 63x magnification. During the analysis phase with ImageJ software, the mean fluorescence intensity (MFI) for each slice was calculated for the markers GFAP, S100A10, C3, IBA-1 and CD86. Background fluorescence was subtracted individually for each marker to obtain corrected MFI values. These values were then normalized and expressed as percentages compared to the control group.

TH/DCC-positive cells were quantified manually from images acquired at 20x magnification using ImageJ software (NIH, Bethesda, MD). Goat anti-TH (1:500, ab317785 Abcam), Rabbit anti-DCC (1:200, GTX134053 Genentech), Donkey anti-goat Alexa Fluor-647 (1:200, Invitrogen A32849), Donkey anti-rabbit Alexa Fluor 488 (1:200, Invitrogen A21206) were used. Cell counting was performed by an investigator blinded to the genotype of the animals. To obtain a representative sampling of the SNp, 30-µm-thick sections were selected at regular intervals along the rostro caudal axis. The analysed sections corresponded to the following anteroposterior coordinates relative to bregma, according to the atlas of Franklin and Paxinos (2001): −2.92, − 3.16, − 3.28, − 3.52, and − 3.64 mm. For each coordinate, sections

from the different experimental groups (WT vs. A53T-α-Syn-Transgenic mice) were matched. Cell counts obtained from individual sections were averaged for each animal and subsequently expressed as a percentage of the corresponding WT control group.

For immunofluorescence analysis on primary astrocytes the cells were fixed in PFA 4%. After washing, they were permeabilized in Triton-X100 0.3% and the blocked in BSA 3%. After incubation with primary (mouse anti-GFAP 1:500, Thermo Fisher Scientific, 14-9892-82; rabbit anti-$G\alpha_o$ 1:200, PA5-3004, Invitrogen, rabbit anti-$G\alpha_o$ 1:200, 3975, Cell Signaling) and appropriate secondary antibodies (goat anti-mouse Alexa Fluor 488 1:500, Invitrogen, A11001 and goat anti-rabbit Alexa Fluor 555 1:200, Invitrogen, A-21428) cells were stained with DAPI (Fluoroshield™ with DAPI, Sigma, F6057-20ML). Acquisition was taken using a confocal microscope (Zeiss LSM 700) with a x63 objective. The fluorescence intensity analysis was performed on primary mesencephalic and striatal astrocytes to semi-quantitatively assess the fluorescence intensity of *Gnao1*, using ImageJ software, following the guidelines provided by Shihan MH[40]. Particularly, the confocal microscope images in lsm format were opened and split into individual channels relative to GFAP, *Gnao1* and DAPI (Image, Colour, Split Channels). GFAP-positive cells were then outlined, and this ROI was applied to the *Gnao1* channel. The mean fluorescence intensity (MFI) was calculated as the sum of all pixel values within the ROI divided by the number of pixels. We compared the ratio MFI/cell area between WT and A53T astrocytes.

Enzyme-linked immunosorbent assay (ELISA)

The intracellular cAMP concentration was analysed using an ELISA kit (CAT. EIA-CAMP-1 Raybiotech) on lysates from wild-type and A53T primary astrocytes, following the manufacturer's protocol. Primary astrocytes were plated in 100 mm petri dishes at a density of 2.2 x 10^6. When the cells reached confluence, they were lysed according to the kit instructions. The supernatant was collected by a centrifugation of 10,000×g for 10 min at 4°C and the cAMP concentration determined according to the manufacturer's instructions. The samples were read at 450nm using the SpectraMax iD5 microplate reader (Molecular Devices).

Molecular biology analysis

Total RNA was isolated from the midbrain and striatum of male WT and A53T-α-Syn-Transgenic mice using the GeneJET RNA Purification Kit following the manufacturer’s protocol (Thermo Scientific™ CAT: K0731). RNA quality and quantification were assessed using a NanoDrop (Thermo Scientific™). 500 ng of RNA was reverse transcribed using High-Capacity cDNA Reverse Transcription Kit (CAT:4368814 Thermo Scientific™) according to the datasheet indications. qRT-PCR was performed to assess the expression of murine *Gnao1* (Mm00494677_m1), CXCL10 (Mm00445235_m1) GFAP (Mm01253033_m1) C3 (Mm01232779_m1) S100a10 (Mm00501457_m1) CD14 (Mm00438094_g1) PTX3 (Mm00477268_m1) AIF-1 (Mm00479862_g1) NOS2(Mm00440502_m1) CD86 (Mm00444540_m1) TNF-α (Mm00443258_m1) CD68 (Mm03047343_m1) C1q (Mm07295529_m1) IL-1β (Mm00434228_m1)

Serping-1 (Mm00437835_m1) Amigo-2(Mm00662105_s1) SOX9 (Mm00448840_m1) CD206 (Mm01329359_m1) using β-Actin (Mm02619580_g1) as the reference gene for normalization. All samples were run in triplicate. For each reaction, 25ng of cDNA was used in a 2X TaqMan™ Fast Advanced Master Mix (Applied Biosystems), in a total volume of 10 µl. The qPCR was conducted using a BioRad CFX Opus Real-Time PCR Systems in standard run mode. Differences in markers levels were calculated using the 2 − ΔΔCt method to calculate Fold Change comparing the threshold cycles between the target genes and the reference gene (β-Actin).

Total cellular RNA was isolated from primary mesencephalic and striatal astrocytes, obtained from WT and A53T-α-Syn-Transgenic pups, by the Quick-RNA Microprep kit following the manufacturer's protocol (Zymo Research). RNA quality control and the quantification was performed with NanoDrop (Thermo Scientific™). 1 µg of RNA was reverse transcribed using High-Capacity cDNA Reverse Transcription Kit (CAT: 4368814 Thermo Scientific™) according to the datasheet. qRT-PCR was performed to assay murine C3 (Mm01232779_m1) S100a10 (Mm00501457_m1) TNF-α (Mm00443258_m1) IL-1β(Mm00434228_m1) Serping-1 (Mm00437835_m1) Amigo-2 (Mm00662105_s1) SOX9 (Mm00448840_m1) *Gnao1* (Mm00494677_m1), with GAPDH (Mm99999915_m1) used for normalization. All samples were run in duplicate. 25ng cDNA was used in 2X master mix, TAQMAN™ Fast Advanced (Applied Biosystems) at a total volume of 10µl. a BioRad CFX Opus Real-Time PCR Systems in standard run mode. Differences in markers levels were calculated using the 2 − ΔΔCt method, comparing the threshold cycles between the target genes and the reference gene (GAPDH).

In silico Analysis

Linear regression model was fitted using the *lm* function from the stats package in R. Genes were considered as deviating from the linear model if their absolute FC difference fell outside the 95th percentile of absolute delta FC. The ggplot2 and ggvenn packages were used for data visualization. Kyoto Encyclopedia of Genes and Genomes (KEGG: http://www.genome.jp/kegg/) was applied for enrichment analysis of genes. gProfiler R package was employed to test the statistical enrichment. KEGG terms with FDR-corrected P-value less than 0.05 were considered significantly enriched. Statistical analyses were performed either in R (version 4.3) or GraphPad with an alpha level set at 0.05.

Small interfering RNA transfection

The *Gnao1* Silencer Select (CAT #4390771–ID s232513), at a 50 nM concentration, was transfected into primary mesencephalic astrocytes using Lipofectamine 2000 (Invitrogen), according to the manufacturer's protocol. After 6 hours, the medium was replaced with fresh medium. The knockdown efficiencies for siRNAs were evaluated by quantitative real-time PCR (48 hours post-transfection) and Western blotting (72 hours post-transfection). Three different siRNAs for *Gnao1* were tested at different concentrations (10, 25, and 50 nM) in WT mesencephalic astrocytes: ID s232512, ID s232513, and ID s66800 (Figure S6C-E). The siRNA ID s232513, which showed the highest knockdown efficiency, was selected for in vitro studies (Figure S6C-D).

LPS Treatment

Mouse mesencephalic astrocytes (DIV14), derived from wild-type (WT) pups, were serum-starved in FBS-free DMEM for 24 hours and subsequently treated with 100 ng/mL LPS for 48 hours.

Statistical analysis

Statistical analysis was carried out using Prism 8 (GraphPad Software, San Diego, CA, USA). Results have been reported as the mean ± standard error of the mean (SEM). The normality of data distribution within each experimental group was assessed using the Shapiro–Wilk test for sample sizes < 8 and the D'Agostino–Pearson omnibus normality test for sample sizes > 8. Comparisons between two groups with normally distributed data were conducted using an unpaired Student's *t*-test. Outliers were identified and excluded using the Robust Regression and Outlier Removal (ROUT) method (Q = 1%) implemented in GraphPad Prism. A p value < 0.05 was considered statistically significant. Detailed information regarding experimental groups and the statistical analyses performed is provided in the corresponding figure legends.

Discussion

The results reported in the present study identify the heterotrimeric G-protein subunit $G\alpha_o$, encoded by the *Gnao1* gene as a novel region-specific regulator of astrocyte activity in the prodromal and intermediate stages of PD pathogenesis in A53T-α-Syn-transgenic mouse model. This aspect is extremely important, considering that $G\alpha_o$ has traditionally been studied for its function in neuronal populations, particularly in MSNs in response to dopaminergic signaling[41]. Interestingly, our findings expand the recognized role of $G\alpha_o$ in cellular signalling, to the glial regulatory mechanisms, suggesting that astrocyte-specific modifications in their functional properties may contribute to the pathogenetic events occurring in the midbrain of A53T-α-Syn-transgenic mice during disease progression. Indeed, although astrocytes from the midbrain and striatum shared a substantial proportion of dysregulated genes in prodromal stages of the disease, *Gnao1* was specific upregulated in mesencephalic astrocytes. This finding highlights the regional specificity of *Gnao1* regulation and prompted us to hypothesize that local and molecular network may shapes astrocyte responses to the stress conditions associated with A53T-α-Syn-transgenic mouse model[42,43]. Evidence indicates that astrocytes are highly heterogeneous across the central nervous system and exhibit region-specific transcriptional identities under both physiological and pathological conditions[44–46]. Our data extend this concept to PD, suggesting that mesencephalic astrocytes can engage a distinct adaptive response characterized by the induction *of Gnao1*-dependent signalling pathways. In this regard, the findings reported in the present study describe a novel and more complex scenario in the current framework of reactive astrocyte function based on evidence demonstrating that the inflammatory astrocyte states are induced by microglial-derived TIC[19–21]. Indeed, in the PD animal model used in the present study, while astrocytes displayed a substantial degree of transcriptional convergence across regions, microglia exhibited highly divergent regional responses and lacked a common dysregulated gene signature. Although these observations do not

exclude microglial contributions to astrocyte activation, they suggest that the observed astrocyte states may reflect the integration of cell-intrinsic regulatory mechanisms and region-specific environmental signals rather than being explained solely by a uniform microglial-activated inflammatory program. In this scenario, the increased of *Gnao1* products expression associated with elevated cAMP levels and the enhanced CREB phosphorylation detected in mesencephalic astrocytes further emphasize this hypothesis. Although these findings might be surprisingly, because $G\alpha_o$ proteins are classically linked to inhibitory G-protein signalling, accumulating evidence indicates that the relationship between $G\alpha_o$ signalling and intracellular cAMP levels is highly context-dependent and may involve receptor-specific coupling, Gβγ-mediated signalling and compensatory feedback mechanisms[47]. Particularly $G\alpha_o$ acts as a key regulator of adenylyl cyclase, the enzyme responsible for cAMP production[41]. This complex system depends on inhibitory and stimulatory inputs. By regulating the dissociation and availability of Gβγ subunits, $G\alpha_o$ indirectly influences downstream signalling events, thereby modulating both inhibitory and stimulatory pathways[41]. Our finding thus supports an association between *Gnao1* upregulation and activation of the cAMP/PKA/CREB signalling, though the molecular mechanisms linking $G\alpha_o$ abundance to cAMP elevation remain to be established, and suggest that CREB may contribute to the regulation of cellular metabolism, trophic support and stress adaptation. Therefore, the activation of this pathway may represent one of the mechanisms through which mesencephalic astrocytes respond to α-synuclein-induced dysfunction. This hypothesis is supported by previous literature describing the neuroprotective role of *Gnao1* in glial cells. First, *Gnao1* plays a key role in diabetic encephalopathy through the cAMP/PKA/CREB/BDNF axis since its downregulation leads to increased reactive oxygen species (ROS) and decreased proliferation in primary astrocytes[48]. Second, *Gnao1* expression in Schwann cells has been shown to promote differentiation through increased cAMP content and activation of the PI3K/AKT pathway[49].

Intriguingly, our functional experiments further support a regulatory role for *Gnao1* in astrocyte state transitions. Specifically, mesencephalic astrocytes isolated from A53T mice retained the expression of markers associated with physiological activation and neurotrophic competence, whereas *Gnao1* downregulation promoted the expression of inflammatory genes and impaired growth factor production. More interestingly the results obtained in WT mesencephalic astrocytes treated with LPS showed a transcriptomic profile similar to the *Gnao1* down-regulation profile, supporting our hypothesis that *Gnao1* might play a role in regulating the astrocytic reactivity.

Together, these findings identify *Gnao1* as more than a passive marker of astrocyte heterogeneity and suggest that it actively contributes to the maintenance of a non-pathological astrocyte phenotype. In this context, *Gnao1* might work as a part of an endogenous compensatory programme that initially counteracts the detrimental consequences of α-synuclein accumulation. The dynamics of glial cells observed in our ex-vivo study in midbrain and striatum of A53T mice further reinforce this interpretation. Indeed, astrocytic alterations emerged at 12 months of age in A53T-α-Syn-Transgenic mice, a time coinciding with the presence of dopaminergic neurons displaying reduced TH expression but preserved DDC levels, a phenotype consistent with a functional impairment in the absence of an evident cellular

loss[50]. Notably, neurodegeneration was only detected in A53T mice at 16 months of age, considered a later stage of disease. Intriguingly, microglial cells in the midbrain of A53T-α-Syn-Transgenic mice failed to respond as demonstrated by the fact that activation markers such as CD68 do not show significant changes. This absence of significant changes in CD68 expression suggests that microglial activation is not prominent at this stage, whereas astrogliosis represents the dominant glial response observed in the midbrain in this model. These observations place astrocytic remodelling as an early adaptive response that may contribute to the support of dopaminergic neurons before substantial neuronal loss occurs. In this regard, the results provided by the present study demonstrated that glial adaptation represent an early driving component in the disease progression rather than a mere consequence of neurodegeneration, in line with previous findings obtained in the same experimental model[37,51] as well as in other α-Syn mouse models of PD[52]. Moreover, these results indicated *Gnao1* as a candidate intracellular regulator of the adaptive signalling response observed in mesencephalic astrocytes. However, whether *Gnao1* dependent astrocyte responses contribute directly to neuronal resilience remains to be established. Nevertheless, the temporal relationship identified in the present study, together with the detrimental astrocytic phenotype induced by *siGnao1*, supports this possibility. Overall, these results lead us to hypothesize that in the midbrain of A53T-α-Syn-Transgenic mice, the extracellular aggregates of α-Syn may activate astrocytic reactivity. The increase of *Gnao1* products, in the early phase of the disease, could serve as a neuroprotective compensatory response aimed to preserve the neurotrophic function of mesencephalic astrocytes.

Several aspects deserve further consideration. First, complementary gain-of-function approaches will be needed to consolidate the causal role of *Gnao1* in mesencephalic astrocytes. Second, future studies combining proteomic and transcriptomic approaches would be useful to identify the direct downstream targets of *Gnao1* activity connecting cAMP/CREB axis to $G\alpha_o$ signalling pathway. Finally, direct assessment of neuron–astrocyte interactions would be instrumental to determine whether *Gnao1*-dependent astrocyte states influence dopaminergic neuron survival. Nevertheless, the convergence of transcriptomic, biochemical and functional evidence reported in the present study strongly suggest a role for *Gnao1* as a regulator of mesencephalic astrocyte responses during PD progression in A53T-α-Syn-Transgenic mice.

Conclusion

This study identifies *Gnao1* as a previously unrecognized regulator of mesencephalic astrocyte responses during PD progression. We show that *Gnao1* is selectively induced in mesencephalic astrocytes before neurodegeneration, where its upregulation is associated with activation of cAMP/PKA/CREB signalling and the maintenance of a physiologically active astrocyte state. Functional silencing experiments demonstrate that *Gnao1* contributes to the preservation of trophic support and restrains inflammatory astrocyte reactivity. These findings reveal a region-specific astrocyte programme that emerges during the early stages of disease progression and suggest that adaptive glial responses may influence the trajectory of neurodegeneration. This has critical relevance from a translational

perspective, as the temporal alignment between this midbrain-specific astrocytic response and neuronal integrity reveals a strategic window for therapeutic intervention. At 12 months, dopaminergic neurons in the SNpc had not yet degenerated; instead, they existed in a "silent" state characterized by a dramatic loss of TH but preserved DDC expression, suggestive of metabolic latency rather than structural death[50]. By 16 months, this compensatory phase failed, leading to complete neurodegeneration with the loss of both markers. Because the peak of astrocytic *Gnao1* upregulation and protective reactivity directly coincides with this 12-month neuronal state, we propose that this astrocytic mechanism may represent an endogenous, region-specific adaptive mechanism that contributes to the maintenance of dopaminergic neuronal function before overt neurodegeneration. In conclusion, our work establishes *Gnao1* as a candidate molecular regulator of astrocyte heterogeneity in PD and provides a framework for exploring glia-centred therapeutic strategies aimed at enhancing endogenous protective mechanisms before irreversible neuronal loss occurs. Future strategies aimed at enhancing or sustaining this astrocytic $G\alpha_o$ signalling cascade may help to determine whether modulation of this endogenous adaptive response can preserve dopaminergic neuronal function and delay neurodegenerative progression.

Declarations

Author information

Authors and Affiliations

Division of Pharmacology, Department of Neuroscience, School of Medicine, University of Naples “Federico II”, Naples, Italy.

Michele Tufano, Rohan Mahesh Patil, Elena D’Apolito, Ester Licastro, Giuseppe Pignataro, Anna Pannaccione, Antonella Scorziello.

Michele Tufano the recipient of a post-doctoral research fellowship funded by the PNRR-MCNTZ-2023-12377900 project.

Department of Translational Medical Sciences, University of Naples “Federico II”, Naples, Italy.

Maria Josè Sisalli

Department of Biomedical Sciences and Public Health, Polytechnic University of Marche, Ancona, Italy.

Agnese Secondo

IRCCS Synlab SDN S.p.A, Via Gianturco 113, Naples, Italy

Lucio Annunziato

Contributions

M.T. and Ant.S. conceived and designed the study. Ant.S. secured funding and supervised the project. M.T. performed all the experiments, collected and analyzed the data, and wrote the manuscript. G.D.R. generated and analyzed the *in-silico* data. R.M.P. performed the *ex vivo* qPCR experiments. E.L. conducted the *Gnao1* silencing experiments, and E.D.P. performed the Western blot analysis. All authors (G.D.R., M.J.S; R.M.P., E.L., E.D.P., G.P., A.P., A.S. L.A. and Ant.S.) contributed to writing, editing and revising the manuscript.

Ethics declarations

The authors declare no competing interests.

Ethical considerations

All experiments were performed following the Guide for the Care and Use of Laboratory Animals and approved by the Animal Care Committee of “Federico II”, University of Naples, Italy, Authorization n° 588/20; 658/24 -PR.

Author Contribution

M.T. and Ant.S. conceived and designed the study. Ant.S. secured funding and supervised the project. M.T. performed all the experiments, collected and analyzed the data, and wrote the manuscript. G.D.R. generated and analyzed the in-silico data. R.M.P. performed the ex vivo qPCR experiments. E.L. conducted the Gnao1 silencing experiments, and E.D.P. performed the Western blot analysis. All authors (G.D.R., M.J.S; R.M.P., E.L., E.D.P., G.P., A.P., A.S. L.A. and Ant.S.) contributed to writing, editing and revising the manuscript.

Acknowledgement

This study was supported by the Italian Ministry of University and Research (MUR) through the PRIN 2022 program (grant number 2022XF7YYI) and the National Recovery and Resilience Plan (PNRR), Project PE12 "MNESYS: A Multiscale Integrated Approach to the Study of the Nervous System in Health and Disease" (DN 1553, 11.10.2022), Spoke 6. This work was also supported by the European Union – NextGenerationEU and the Italian Ministry of Health under the PNRR (M6C2 - Investment 2.1: Strengthening and enhancing biomedical research of the National Health Service), project number PNRR-MCNTZ-2023-12377900, titled “Development and validation of a panel of easily-accessible diagnostic and prognostic biofluid biomarkers of synucleinopathies”. All grants are awarded to Ant.S.. M.T. is a post-doctoral research fellow funded by this grant. PRIN 2022 grant number 2022LZWMX5 To MJS.

References

1. Feng, H., Khalil, S., Neubig, R. R. & Sidiropoulos, C. A mechanistic review on GNAO1-associated movement disorder. *Neurobiol. Dis.* 116, 131–141 (2018).
2. Solis, G. P. *et al.* Pediatric Encephalopathy: Clinical, Biochemical and Cellular Insights into the Role of Gln52 of GNAO1 and GNAI1 for the Dominant Disease. *Cells* 10, (2021).
3. Muntean, B. S. *et al.* Gαo is a major determinant of cAMP signaling in the pathophysiology of movement disorders. *Cell Rep.* 34, (2021).
4. Jiang, M. *et al.* Multiple neurological abnormalities in mice deficient in the G protein Go. *Proc. Natl. Acad. Sci. U. S. A.* 95, 3269–3274 (1998).
5. Ryan, M. B., Bair-Marshall, C. & Nelson, A. B. Aberrant Striatal Activity in Parkinsonism and Levodopa-Induced Dyskinesia. *Cell Rep.* 23, 3438–3446.e5 (2018).
6. Zhai, S., Shen, W., Graves, S. M. & Surmeier, D. J. Dopaminergic modulation of striatal function and Parkinson's disease. *J. Neural Transm. (Vienna)* 126, 411 (2019).
7. Novelli, M. *et al.* GNAO1-related movement disorder: An update on phenomenology, clinical course, and response to treatments. *Parkinsonism Relat. Disord.* 111, (2023).
8. Lasa-Aranzasti, A. *et al.* Clinical and Molecular Profiling in GNAO1 Permits Phenotype-Genotype Correlation. *Mov. Disord.* 39, 1578–1591 (2024).
9. Schirinzi, T. *et al.* Phenomenology and clinical course of movement disorder in GNAO1 variants: Results from an analytical review. *Parkinsonism Relat. Disord.* 61, 19–25 (2019).
10. Domínguez-Carral, J. *et al.* Severity of GNAO1-Related Disorder Correlates with Changes in G-Protein Function. *Ann. Neurol.* 94, 987–1004 (2023).
11. Kim, S. Y. *et al.* Spectrum of movement disorders in GNAO1 encephalopathy: in-depth phenotyping and case-by-case analysis. *Orphanet J. Rare Dis.* 15, (2020).
12. Solis, G. P. *et al.* GNAO1 Mutations Affecting the N-Terminal α-Helix of Gαo Lead to Parkinsonism. *Mov. Disord.* 39, 601–606 (2024).
13. Zhong, J. *et al.* Single-cell brain atlas of Parkinson's disease mouse model. *Journal of Genetics and Genomics* 48, 277–288 (2021).
14. Xu, S., Yu, W., Zhang, X., Wang, W. & Wang, X. The regulatory role of Gnao1 protein in diabetic encephalopathy in KK-Ay mice and streptozotocin-induced diabetic rats. *Brain Res.* 1792, (2022).
15. Xu, J. *et al.* The Schwann cell-specific G-protein Gαo (Gnao1) is a cell-intrinsic controller contributing to the regulation of myelination in peripheral nerve system. *Acta Neuropathol. Commun.* 12, 24 (2024).
16. Liddelow, S. A. *et al.* Neurotoxic reactive astrocytes are induced by activated microglia. *Nature* 541, 481–487 (2017).
17. Guttenplan, K. A. *et al.* Knockout of reactive astrocyte activating factors slows disease progression in an ALS mouse model. *Nat. Commun.* 11, (2020).

18. Hill, E. J. *et al.* Temporal regulation of human reactive astrocytes reveals their capacity for antigen presentation. *Neuron* 114, (2026).
19. Liddelow, S. A. *et al.* Neurotoxic reactive astrocytes are induced by activated microglia. *Nature* 541, 481–487 (2017).
20. Guttenplan, K. A. *et al.* Knockout of reactive astrocyte activating factors slows disease progression in an ALS mouse model. *Nat. Commun.* 11, (2020).
21. Hill, E. J. *et al.* Temporal regulation of human reactive astrocytes reveals their capacity for antigen presentation. *Neuron* 114, (2026).
22. Zamanian, J. L. *et al.* Genomic analysis of reactive astrogliosis. *J. Neurosci.* 32, 6391–6410 (2012).
23. Anderson, M. A. *et al.* Astrocyte scar formation aids central nervous system axon regeneration. *Nature* 532, 195–200 (2016).
24. McKeon, R. J., Schreiber, R. C., Rudge, J. S. & Silver, J. Reduction of neurite outgrowth in a model of glial scarring following CNS injury is correlated with the expression of inhibitory molecules on reactive astrocytes. *J. Neurosci.* 11, 3398–3411 (1991).
25. Fitch, M. T. & Silver, J. CNS injury, glial scars, and inflammation: Inhibitory extracellular matrices and regeneration failure. *Exp. Neurol.* 209, 294–301 (2008).
26. Alilain, W. J., Horn, K. P., Hu, H., Dick, T. E. & Silver, J. Functional regeneration of respiratory pathways after spinal cord injury. *Nature* 475, 196–200 (2011).
27. Brambilla, R. *et al.* Inhibition of astroglial nuclear factor kappaB reduces inflammation and improves functional recovery after spinal cord injury. *J. Exp. Med.* 202, 145–156 (2005).
28. Brambilla, R. *et al.* Transgenic Inhibition of Astroglial NF-κB Improves Functional Outcome in Experimental Autoimmune Encephalomyelitis by Suppressing Chronic Central Nervous System Inflammation. *J. Immunol.* 182, 2628 (2009).
29. Bush, T. G. *et al.* Leukocyte infiltration, neuronal degeneration, and neurite outgrowth after ablation of scar-forming, reactive astrocytes in adult transgenic mice. *Neuron* 23, 297–308 (1999).
30. Faulkner, J. R. *et al.* Reactive astrocytes protect tissue and preserve function after spinal cord injury. *J. Neurosci.* 24, 2143–2155 (2004).
31. Voskuhl, R. R. *et al.* Reactive astrocytes form scar-like perivascular barriers to leukocytes during adaptive immune inflammation of the CNS. *J. Neurosci.* 29, 11511–11522 (2009).
32. Yang, H. M., Wang, Y. L., Liu, C. Y., Zhou, Y. T. & Zhang, X. F. A time-course study of microglial activation and dopaminergic neuron loss in the substantia nigra of mice with paraquat-induced Parkinson's disease. *Food and Chemical Toxicology* 164, (2022).
33. Plastira, I. *et al.* 1-Oleyl-lysophosphatidic acid (LPA) promotes polarization of BV-2 and primary murine microglia towards an M1-like phenotype. *J. Neuroinflammation* 13, (2016).
34. Mirarchi, A., Albi, E. & Arcuri, C. Microglia Signatures: A Cause or Consequence of Microglia-Related Brain Disorders? *International Journal of Molecular Sciences 2024, Vol. 25, Page 10951* 25, 10951 (2024).

35. Boddaert, J. *et al.* CD8 signaling in microglia/macrophage M1 polarization in a rat model of cerebral ischemia. *PLoS One* 13, e0186937 (2018).
36. Heo, J. Y. *et al.* Aberrant Tonic Inhibition of Dopaminergic Neuronal Activity Causes Motor Symptoms in Animal Models of Parkinson's Disease. *Curr. Biol.* 30, 276–291.e9 (2020).
37. Di Martino, R. *et al.* Ncx3-Induced Mitochondrial Dysfunction in Midbrain Leads to Neuroinflammation in Striatum of A53t-α-Synuclein Transgenic Old Mice. *Int. J. Mol. Sci.* 22, (2021).
38. De Risi, M. *et al.* Altered heparan sulfate metabolism during development triggers dopamine-dependent autistic-behaviours in models of lysosomal storage disorders. *Nature Communications 2021 12:1* 12, 3495- (2021).
39. Paxinos, George. & Franklin, K. B. J.. Paxinos and Franklin's The mouse brain in stereotaxic coordinates. https://books.google.com/books/about/Paxinos_and_Franklin_s_the_Mouse_Brain_i.html?id=x3aQDwAAQBAJ (2019).
40. Shihan, M. H., Novo, S. G., Le Marchand, S. J., Wang, Y. & Duncan, M. K. A simple method for quantitating confocal fluorescent images. *Biochem. Biophys. Rep.* 25, (2021).
41. Muntean, B. S. *et al.* Gαo is a major determinant of cAMP signaling in the pathophysiology of movement disorders. *Cell Rep.* 34, (2021).
42. Sirabella, R. *et al.* NCX1 and NCX3 as potential factors contributing to neurodegeneration and neuroinflammation in the A53T transgenic mouse model of Parkinson's Disease. *Cell Death Dis*. 9, (2018).
43. Martino, R. Di *et al.* Ncx3-Induced Mitochondrial Dysfunction in Midbrain Leads to Neuroinflammation in Striatum of A53t-α-Synuclein Transgenic Old Mice. *Int. J. Mol. Sci.* 22, (2021).
44. Endo, F. *et al.* Molecular basis of astrocyte diversity and morphology across the CNS in health and disease. *Science* 378, (2022).
45. Hasel, P., Rose, I. V. L., Sadick, J. S., Kim, R. D. & Liddelow, S. A. Neuroinflammatory astrocyte subtypes in the mouse brain. *Nat. Neurosci.* 24, 1475–1487 (2021).
46. Clayton, B. L. L. *et al.* A phenotypic screening platform for identifying chemical modulators of astrocyte reactivity. *Nature Neuroscience 2024 27:4* 27, 656–665 (2024).
47. Durkee, C. A. *et al.* Gi/o protein-coupled receptors inhibit neurons but activate astrocytes and stimulate gliotransmission. *Glia* 67, 1076–1093 (2019).
48. Xu, S., Yu, W., Zhang, X., Wang, W. & Wang, X. The regulatory role of Gnao1 protein in diabetic encephalopathy in KK-Ay mice and streptozotocin-induced diabetic rats. *Brain Res.* 1792, (2022).
49. Xu, J. *et al.* The Schwann cell-specific G-protein Gαo (Gnao1) is a cell-intrinsic controller contributing to the regulation of myelination in peripheral nerve system. *Acta Neuropathol. Commun.* 12, 24 (2024).
50. Heo, J. Y. *et al.* Aberrant Tonic Inhibition of Dopaminergic Neuronal Activity Causes Motor Symptoms in Animal Models of Parkinson's Disease. *Curr. Biol.* 30, 276–291.e9 (2020).

51. Sirabella, R. *et al.* NCX1 and NCX3 as potential factors contributing to neurodegeneration and neuroinflammation in the A53T transgenic mouse model of Parkinson's Disease. *Cell Death Dis*. 9, (2018).
52. Basurco, L. *et al.* Microglia and astrocyte activation is region-dependent in the α-synuclein mouse model of Parkinson's disease. *Glia* 71, 571–587 (2023).

Figures

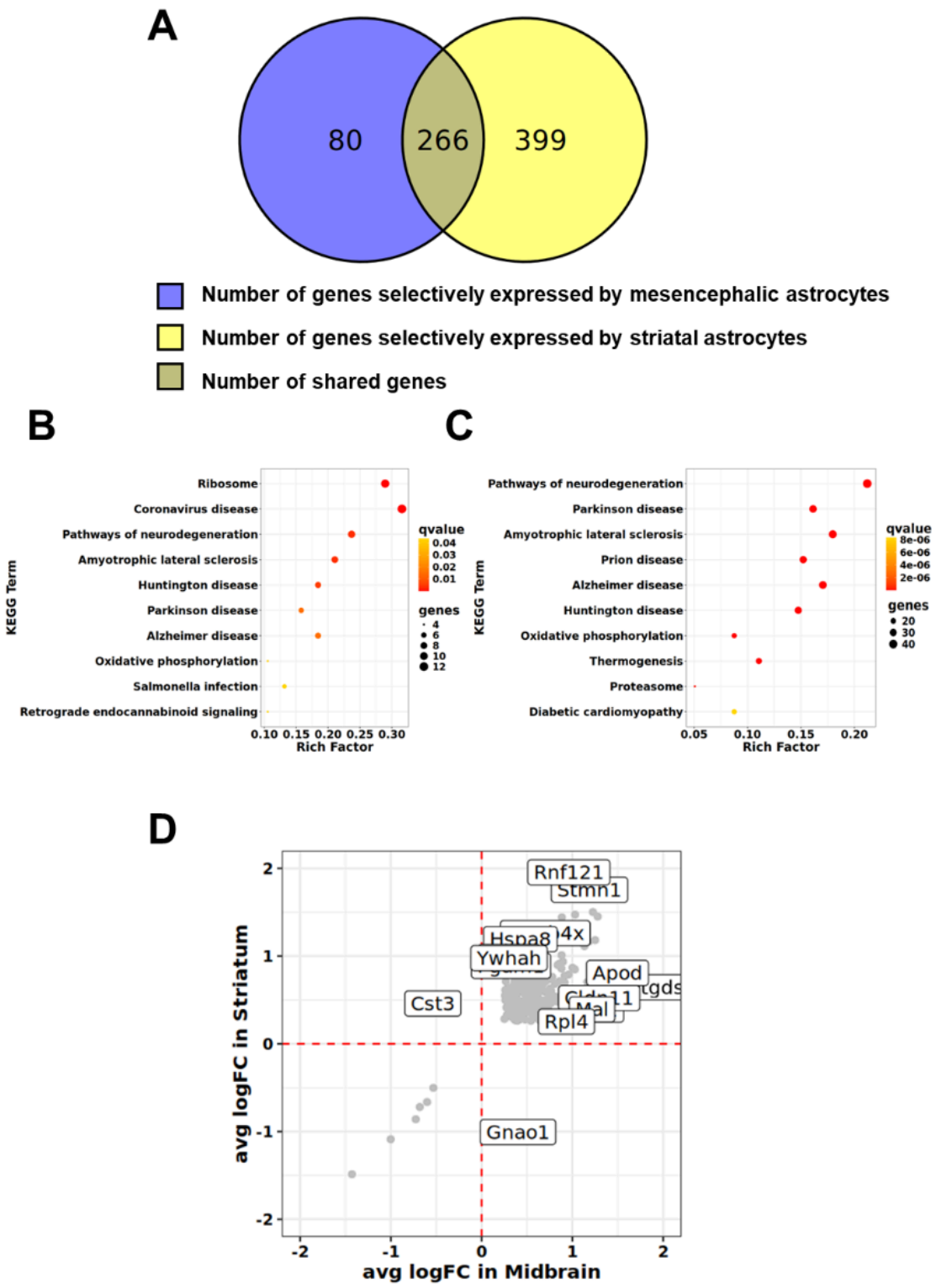


Figure 1

***Gnao1* is selectively upregulated in A53T-α-Syn-Transgenic mesencephalic astrocytes.** (A)The Venn diagram displaying the count of genes selectively altered in respect to WT and overlapping between striatal astrocytes (Yellow) and mesencephalic astrocytes (Blue). 399 genes were altered specifically in striatal astrocytes and 80 unique genes in mesencephalic astrocytes. 266 genes are commonly expressed between these two cell populations. (B-C) Bubble plot presenting the KEGG pathway

enrichment analysis of the 80 and 399 selectively expressed genes in mesencephalic and striatal astrocytes, identifying the associated pathways. The X-axis displays the rich factor derived from enriched KEGG analysis, while the Y-axis indicates the pathway terms. The terms are ordered based on the FDR-adjusted p-value. The bubble size is proportional to gene ratio, i.e. the number of genes contributing to the enrichment out of the number of genes in the considered term. Bubble colour is instead proportional to the level of significance quantified by the adjusted p-value. (D) The dot plot represents the correlation of Fold Change values for the 266 genes commonly expressed between mesencephalic and striatal astrocytes. The X-axis shows the Fold Change values for mesencephalic astrocytes, while the Y-axis displays the Fold Change values for striatal AST. astrocytes Data reanalyzed from Jixing Zhong et al., 2021.

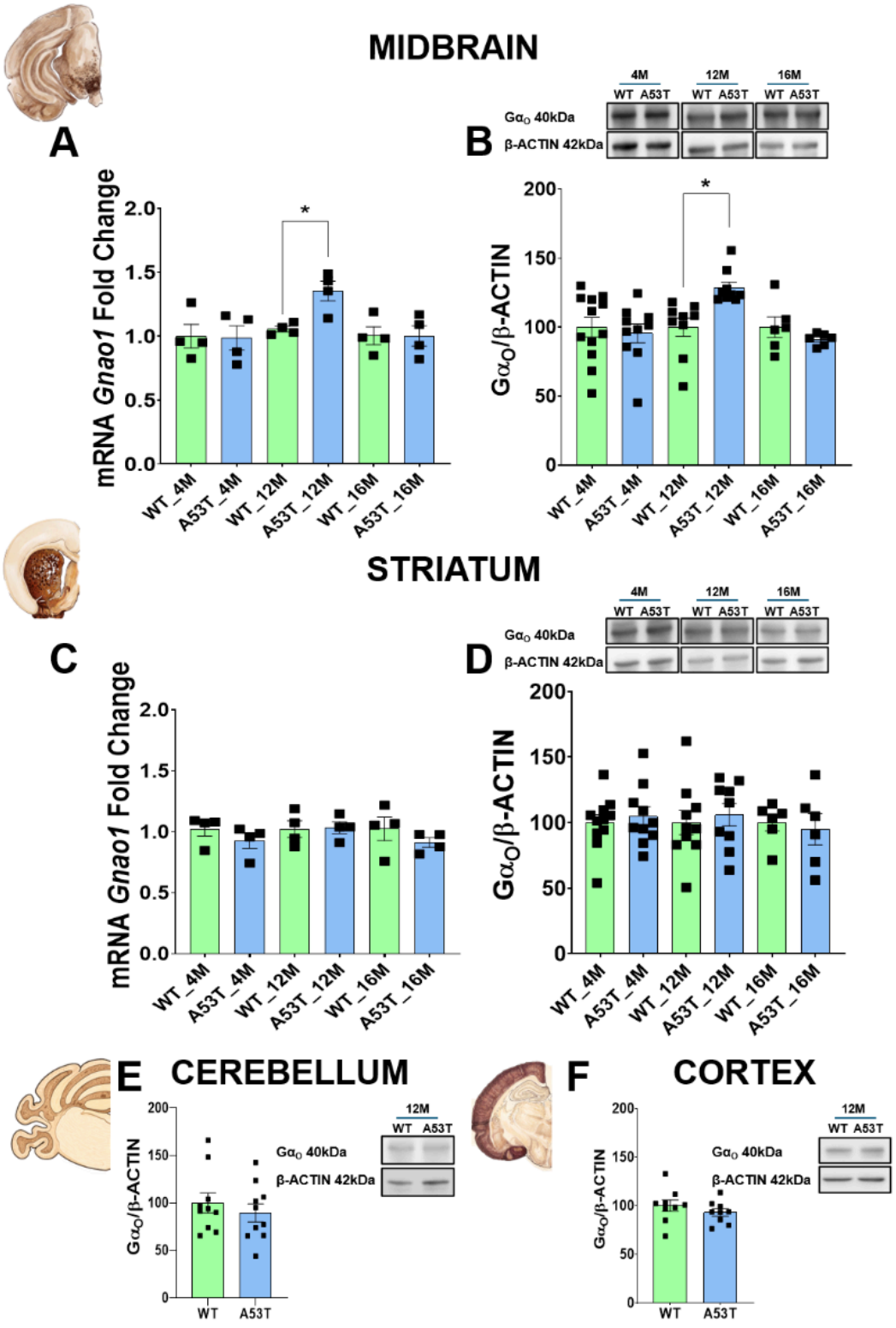


Figure 2

***Gnao1* products are upregulated in the midbrain of 12-month-old A53T-α-Syn-Transgenic mice.** Analysis of *Gnao1* expression in the midbrain of the ex vivo mouse model by qPCR (A) and Western blotting (B). (C-D) qPCR and Western blot analysis of *Gnao1* in striatal of ex vivo mouse model. (E–F) Analysis of *Gnao1*protein expression in the cerebellum (E) and cortex (F) by Western blotting. Data are presented as mean ± SEM relative to control mice. Statistical significance was determined by One-way

ANOVA followed by Tukey's multiple comparisons test for qPCR analysis, and by Holm-Sidak's test for Western blot analysis (*p< 0.05).

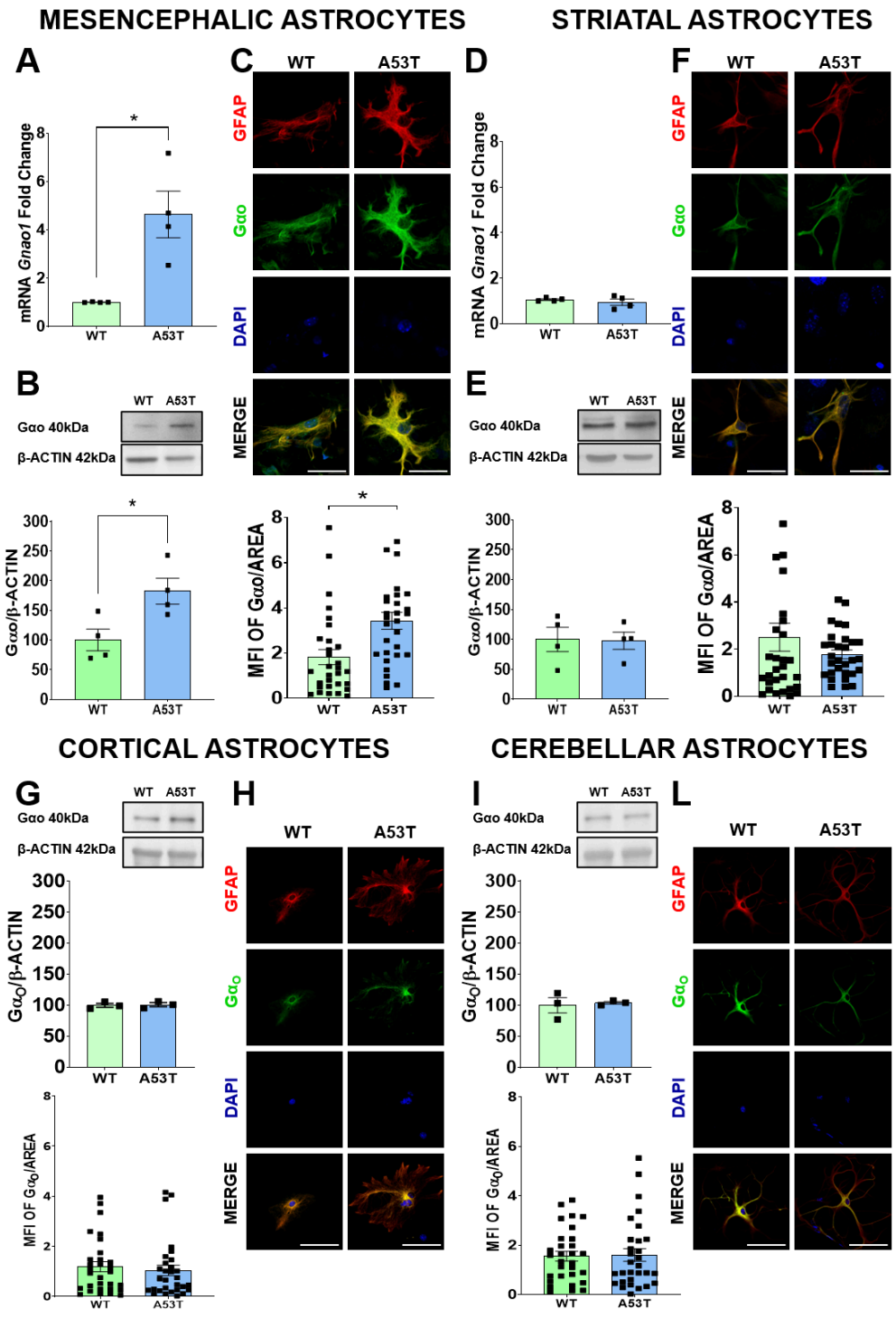


Figure 3

Characterization of *Gnao1* products expression in primary astrocytes isolated from distinct brain regions of WT and A53T-α-Syn-Transgenic mice model. (A) qPCR analysis in primary mesencephalic

astrocytes. Data represent means ± SEM from four independent astrocyte isolations, each performed in duplicate. Statistical analysis was performed using a two-tailed, Unpaired Student's t-test (*p<0.05 vs. WT control; t=3.775; df=6). (B) Western blot analysis in primary mesencephalic astrocytes. Data represent means ± SEM and expressed as % compared to WT from four independent experiments. Statistical analysis was performed using a two-tailed, Unpaired Student's t-test (*p<0.05 vs. WT control; t=2.895, df=6). (C) Immunofluorescence analysis of primary mesencephalic astrocytes. Representative images from four independent experiments are shown (n=30 astrocytes per group; scale bar= 20 μm). Statistical analysis was performed using a two-tailed, Unpaired Student's t-test (*p<0.05 vs. WT; t=3.185, df=58). (D-E-F) qPCR, Western blot, and immunofluorescence analyses (scale bar, 20 μm) of *Gnao1* expression in primary striatal astrocytes. Values represent means ± SEM derived from four independent experiments. (G-H-I-L) Western blot and immunofluorescence analyses (scale bar, 20 μm) of *Gnao1* expression in primary cortical and cerebellar astrocytes isolated from WT and A53T transgenic pups. Data were collected from three independent experimental session.

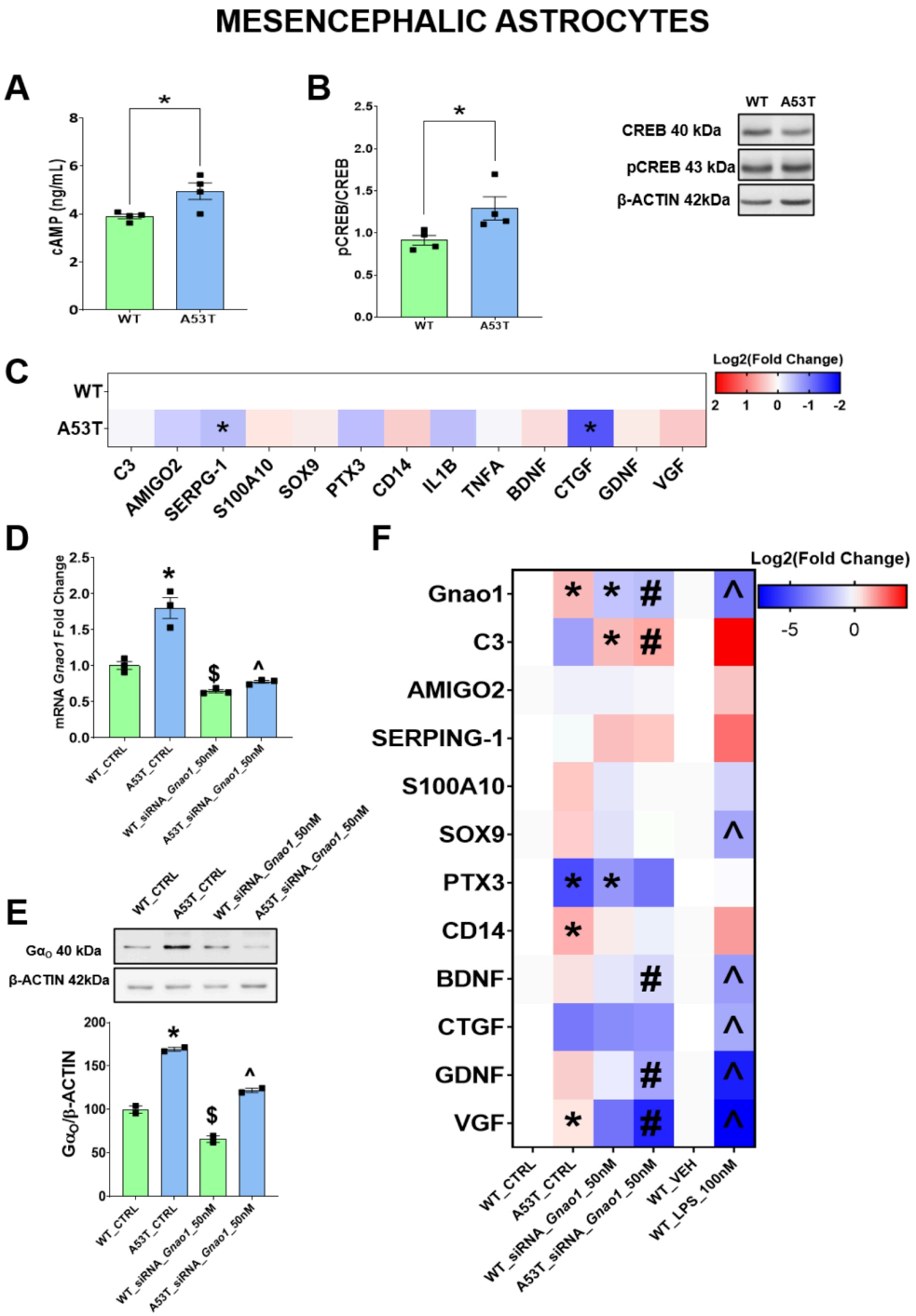


Figure 4

In A53T-α-Syn-Transgenic mesencephalic astrocytes, *Gnao1* regulates cell activation and growth factor expression via cAMP/pCREB signaling. (A-B) Total intracellular cAMP levels and Western blot analysis of CREB and phosphorylated CREB (p-CREB) in primary mesencephalic astrocytes isolated from WT and A53T P0 pups. Data represent values obtained from four independent experimental sessions. Statistical analysis was performed using an Unpaired Student's t-test; a p value <0.05 was considered statistically

significant. *P<0.05 versus WT. (C) Heatmap showing Log_2 fold-change values of genes associated with physiological and pathological astrocyte reactivity. Rows correspond to WT and A53T mesencephalic astrocytes, whereas columns represent individual genes. Log_2-transformed values were used for visualization, while statistical analyses were performed on fold-change values calculated versus WT controls using the 2^−ΔΔCt method. (D–E) qPCR and Western blot analyses of WT astrocytes, A53T astrocytes, and astrocytes transfected with *Gnao1*siRNA. For qPCR analysis data were obtained from three independent experimental sessions each performed in triplicate. Western blot analysis data were collected from two independent experimental sessions. Statistical analysis was performed using an Unpaired Student's *t*-test. *P*<0.05 was considered statistically significant (*p<0.05 vs. WT_CTRL; $p<0.05 WT vs. WT_siRNA_*Gnao1*_50nM; ^p<0.05 A53T_CTRL vs. A53T_siRNA_*Gnao1*_50nM). (F) Heatmap showing the expression of genes associated with pro-inflammatory and anti-inflammatory astrocyte phenotypes in control and *Gnao1* siRNA-treated cells or WT mesencephalic astrocytes treated with LPS 100nM. Rows represent individual genes, whereas columns correspond to the experimental groups: WT, A53T, WT + siRNA_*Gnao1*, and A53T + siRNA_*Gnao1*. Statistical analysis was performed using an Unpaired Student's *t*-test. *P*<0.05 was considered statistically significant (*p<0.05 WT_CTRL vs. WT_siRNA_*Gnao1*_50nM; # p<0.05 A53T_CTRL vs. A53T_siRNA_*Gnao1*_50nM; ^p<0.05 WT_vehicle vs. WT_LPS_100 nM).

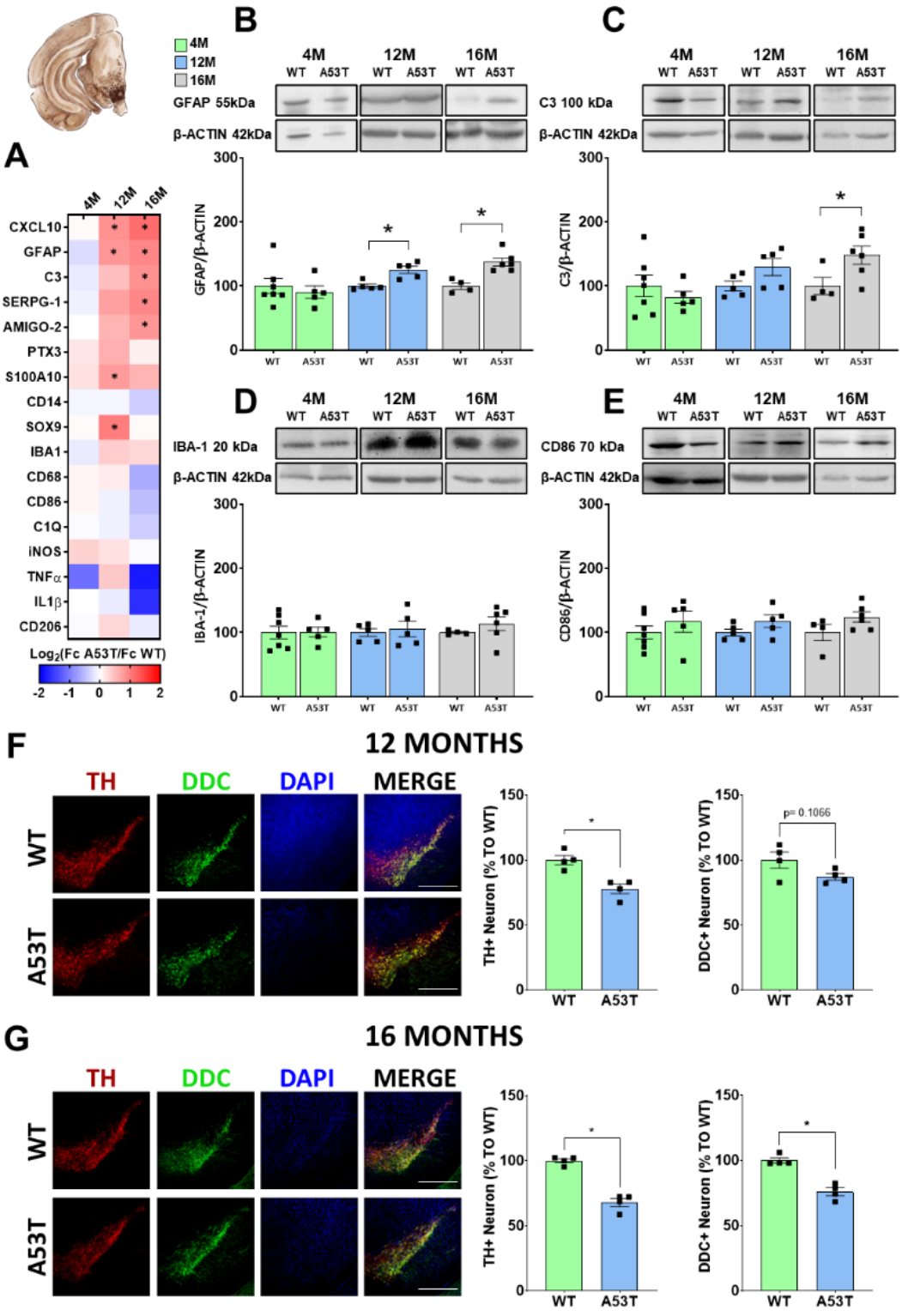


Figure 5

Reactive Gliosis Prevails in the Midbrain of A53T-α-Syn-Transgenic Mice. (A) Real time PCR analysis. Heatmaps compare the Log_2(Fold change A53T/Fold change WT) of pan-reactive, detrimental, and neuroprotective gene transcripts to identify the glial sub-populations in the midbrain at different time points. Data are expressed as ratio of the Fold change observed in A53T mice compared to that observed in WT mice and presented as mean

±
SEM compared to the control mice. Unpaired Student's t-test *p<0.05 (4 months aged mice: WT=4, A53T= 4; 12 months aged mice: WT= 4, A53T= 4; 16 months aged mice: WT= 4, A53T= 4). (B-C-D-E) GFAP, C3, IBA-1 and CD86 protein expression in the midbrain of 4-12-16 months-old-A53T-α-Syn-Transgenic and WT mice. Data are expressed as mean
±
SEM. Unpaired Student's t-test (*p<0.05). (F-G) Representative images of immunofluorescence analysis against TH and DDC in midbrain, scale bar: 100 µm; Unpaired Student's t-test (*p<0.05).

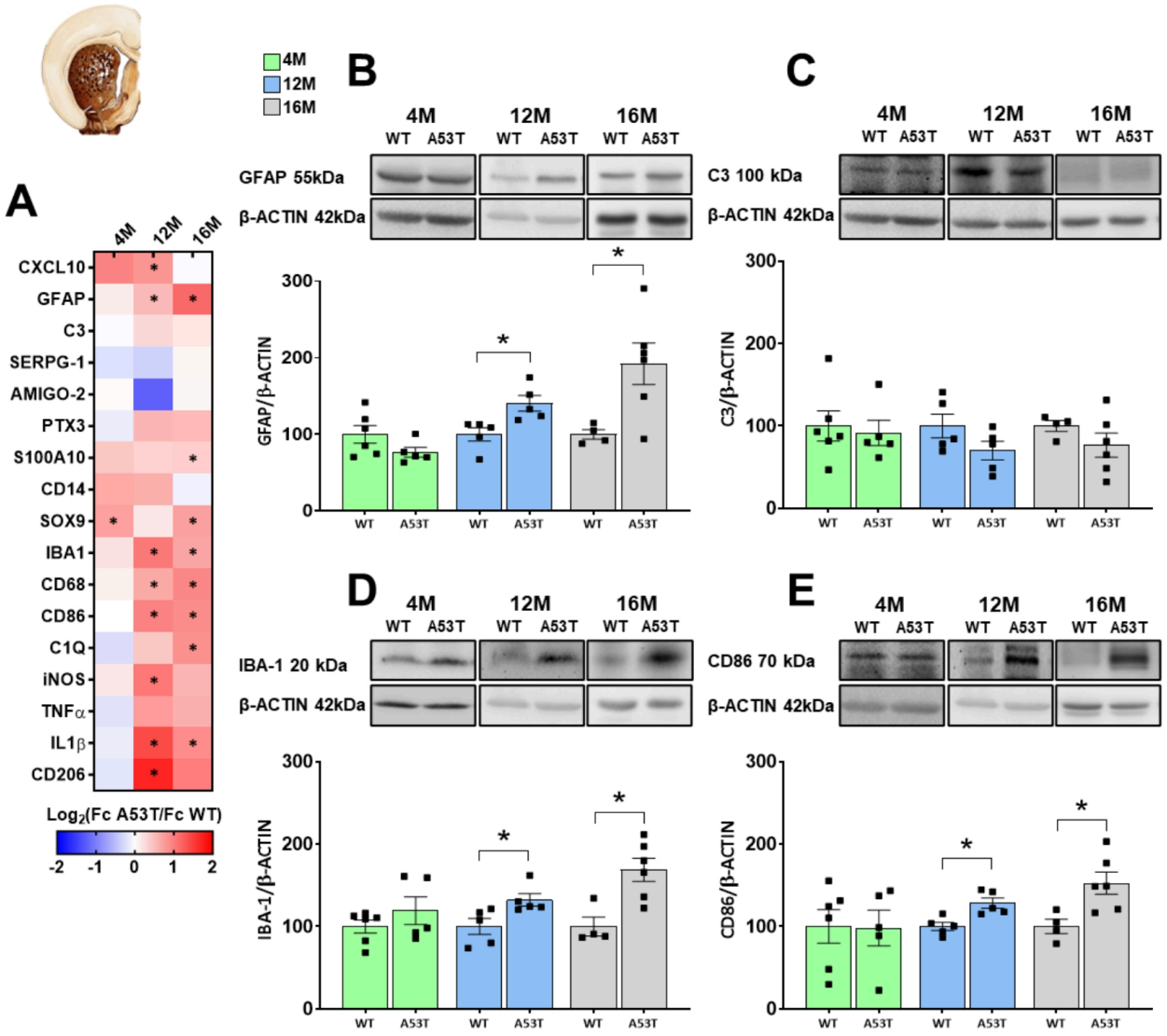


Figure 6

Detrimental microglial cells dominate in the Striatum of A53T-α-Syn-Transgenic Mice. (A) Heatmaps display the Log_2(Fold change A53T/Fold change WT) values of pan-reactive, detrimental, and

neuroprotective gene transcripts to characterize glial subpopulations in the striatum at various time points. Data are expressed as ratio of the Fold change observed in A53T mice compared to that observed in WT mice and presented as mean ± SEM relative to control mice. Unpaired Student’s t-test, *p<0.05 (4-month-old mice: WT=4, A53T=4; 12-month-old mice: WT=4, A53T=4; 16-month-old mice: WT=4, A53T=4). (B-C-D-E) Protein levels of GFAP, C3, IBA-1 and CD86 in the striatum of A53T-α-Syn-Transgenic and WT mice aged 4, 12, and 16 months. Results are shown as mean ± SEM. Unpaired Student's t-test (*p<0.05).

Supplementary Files

This is a list of supplementary files associated with this preprint. Click to download.

- SupplementalMaterialsTufanoetal..docx